Catalysis Today 172 (2011) 209–217

Contents lists available at ScienceDirect

Catalysis Today

journal homepage: www.elsevier.com/locate/cattod

$Ru/La_2O_3–SiO_2$ catalysts for hydrogen production in membrane reactors

B.M. Faroldi, E.A. Lombardo, L.M. Cornaglia *

Instituto de Investigaciones en Catálisis y Petroquímica (FIQ, UNL-CONICET), Santiago del Estero 2829, 3000 Santa Fe, Argentina

ARTICLE INFO

Article history:
Received 1 December 2010
Received in revised form 4 February 2011
Accepted 14 February 2011
Available online 31 March 2011

Keywords:
Methane combined reforming
Ruthenium
$La_2O_3–SiO_2$
Hydrogen production
Membrane reactor

ABSTRACT

Binary $La_2O_3–SiO_2$ supports were employed to obtain active, stable Ru catalysts with high dispersions for the dry reforming of methane. Supports with 15, 27, 40 and 50 wt.% of La_2O_3 were prepared by incipient wetness impregnation of $La(NO_3)_3$ on SiO_2. The Ru loading was 0.6 wt.% for all catalysts.

The solids were evaluated in a fixed-bed reactor under differential conditions. Previously, they were reduced at 550 °C. All the formulations were stable for at least 100 h on stream. Subsequently, the most active catalyst ($Ru/La_2O_3(50)–SiO_2$) was tested in a membrane reactor using different feed mixtures with and without O_2. The reactor configuration was formed by a fixed-bed reactor followed by a membrane reactor. The methane conversion increased when the CO_2/CH_4 ratio increased from 1.0 to 1.9 and when oxygen was added to the feed. Operating under conditions of combined reforming (oxygen addition) and CO_2/CH_4 ratio equal to 1, a high production of hydrogen was also achieved in the membrane reactor.

1. Introduction

The efficient use of the greenhouse gases, CH_4 and CO_2, is a central issue in heterogeneous catalysis. The reaction between these gases for the production of synthesis gas is an attractive alternative to use them simultaneously, contributing to the reduction of emissions to the environment [1,2]. However, this reaction is highly endothermic and is limited by thermodynamic equilibrium. When the goal is to produce high purity hydrogen for use in a fuel cell, these reactions can be carried out in membrane reactors that combine reaction and separation processes in a single device. The membrane reactor allows improving the performance with respect to hydrogen [3–5]. This reactor requires the use of catalysts that are active, stable and do not form carbonaceous residues as this would cause catalyst deactivation and deterioration of the membrane.

Several articles have lately appeared on membrane reactors for the methane dry reforming reaction employing different types of membranes and catalysts [3–6]. In our group, we employed a dense Pd/Ag membrane with 100% selectivity towards hydrogen to produce ultrapure hydrogen and also compared the behavior of different La-based noble metal catalysts in a membrane reactor [3,4,7]. The best performing formulation was obtained using Rh supported on a binary $La_2O_3–SiO_2$ support [8].

The practical usefulness of this reaction could be increased by coupling this process with an exothermic reaction such as the partial oxidation of methane (POM). By combining these reactions and varying the concentrations of O_2 and CO_2, the H_2/CO ratios could evolve to increase the profitability of the process.

Several contributions have studied the combined reaction of methane in fixed-bed or fluidized-bed reactors with Ni [9–11] and Pt [12] catalysts. However, few experimental studies using methane reforming reactions and partial oxidation coupled in a membrane reactor can be found in the literature [13,14].

Due to the coexistence of exothermic and endothermic reactions with rather different kinetics, a non-uniform temperature profile develops in the catalyst bed, with a pronounced hot spot in its uppermost part, where the highest thermal stress is concentrated [15]. Consequently, an adequate design of the catalyst bed is required in order to avoid the rapid deterioration of the membrane [13].

The aim of the present work was to study Ru catalysts supported on $La_2O_3–SiO_2$. These lanthanum based solids were characterized by several techniques and evaluated in a conventional fixed-bed reactor. The best catalyst ($Ru/La_2O_3(50)–SiO_2$) was tested in a membrane reactor for the combined dry reforming and oxidation of methane reactions. We employed different feed compositions with and without O_2, seeking to increase methane conversion and H_2 production.

2. Experimental

2.1. Catalyst preparation

$La_2O_3(X)–SiO_2$ supports were prepared by incipient wetness impregnation of SiO_2 (Aerosil 200, calcined at 900 °C) with lanthanum nitrate (Aldrich 99.9%). Supports with 15, 27, 40 and

* Corresponding author. Tel.: +54 342 4536861; fax: +54 342 4571162.
E-mail address: lmcornag@fiq.unl.edu.ar (L.M. Cornaglia).

0920-5861/$ – see front matter © 2011 Elsevier B.V. All rights reserved.
doi:10.1016/j.cattod.2011.02.039

50 wt.% of La_2O_3 were prepared (nominal values). These values are indicated between parentheses. The samples were kept at room temperature for 2 h and then dried at 80 °C overnight. The supports were calcined for 6 h at 550 °C in flowing air. Metal deposition was performed by incipient wetness impregnation with $RuCl_3{\cdot}3H_2O$ (Alfa Aesar 99.9%) as precursor compound followed by a drying step at 80 °C. The amount of hydration water in the $RuCl_3$ was determined by thermogravimetric analysis. The nominal Ru loading was 0.6 wt.% for all catalysts.

2.2. Catalyst characterization

2.2.1. Surface area

The BET (Brunauer, Emmett, and Teller) surface area was calculated from N_2 adsorption isotherms at liquid nitrogen temperature using a Quantachrome Autosorb automatic gas adsorption instrument. Prior to the measurements, all samples were degassed at 150 °C under a 0.13 Pa overnight.

2.2.2. Metal dispersion

The metal dispersion of the fresh catalyst, following the hydrogen reduction at 550 °C for 1 h, was determined by static equilibrium adsorption of either H_2 at 100 °C or CO at 25 °C in a conventional vacuum system.

The volumetric adsorption measurements were carried out in a conventional glass vacuum apparatus. About 100 mg of the catalyst was placed in a quartz cell, degassed for 1 h at RT, then reduced in H_2 flux at 550 °C for 1 h and evacuated at the same temperature for 1 h. Next, the sample was cooled under vacuum to the adsorption temperature. Adsorption isotherms were measured at 25 °C to CO and 100 °C to H_2, with exposure times varying between 10 min and 4 h. After the first isotherm was recorded, the adsorption cell was outgassed for 10 min at adsorption temperature and a second isotherm was measured. The amount of irreversibly adsorbed hydrogen/CO was determined by assessing the difference between the isotherms. The pressure range of the isotherms was 0.13–2 kPa and the extrapolation to zero pressure was taken as a measure of the hydrogen uptake on the metallic phase.

2.2.3. Thermogravimetric analysis

The amount of hydration water in $RuCl_3$ was determined in a Mettler Toledo TGA/SDTA (Model 851) system. The solid was heated at 10 K min^{-1} to 1173 K in a flow of 90 ml min^{-1} air.

2.2.4. Membrane characterization

The H_2 permeation through the Pd/Ag membrane was measured using a membrane reactor in a temperature range of 400–550 °C and a trans-membrane pressure of 20 kPa.

The reactor filled with quartz wool was heated in Ar flow to 400 °C, and then the feed was switched to pure hydrogen. Afterwards, the same procedure was carried out for the different temperatures under study.

2.3. Catalytic test

2.3.1. Differential fixed-bed reactor

The catalyst was loaded into a tubular quartz reactor (inner diameter, 5 mm) which was placed in an electric oven. The catalyst (10–30 mg) was diluted with 50 mg of inert powder quartz in order to avoid temperature gradients. A thermocouple in a quartz sleeve was placed on top of the catalyst bed. The catalysts were heated up to 550 °C in Ar flow and then reduced in H_2 flow at the same temperature for 2 h.

After reduction, the reactant gas mixture ($P_{CO_2} : P_{CH_4} : P_{Ar} = 1 : 1 : 1.2$, $P = 1$ atm, $W/F = 4.5 \times 10^{-6}$ g h ml^{-1}) was fed to the reactor. The reaction rate measurements under differential conditions were conducted in a conventional flow system. The reaction experiments were carried out at 550 °C. Flows expressed in ml min^{-1} were measured at normal pressure and temperature conditions.

2.3.2. Membrane reactor

The double tubular membrane reactor was built using a commercial dense Pd–Ag alloy (thickness = 50 μm, inner tube), provided by REB Research and Consulting, with one end closed and an inner tube to allow Ar sweep gas flow (SG). Two different membranes (M1 and M2) were used. The outer tube was made of commercial non-porous quartz (i.d. 9 mm). The catalyst (1.5 g), diluted with quartz chips (8 or 10 g), was packed in the outer annular region (shell side), leading to a permeation area of 4 or 6 cm^2. In addition, part of the catalyst bed was placed 0.8 cm above the membrane to prevent its deterioration when exposed to the presence of O_2, leading to a reactor configuration formed by a fixed-bed reactor followed by a membrane reactor. More details are given elsewhere [13]. The inner side of the membrane in all runs was kept at atmospheric pressure. The catalysts were heated up to 550 °C in Ar flow and then reduced in H_2 flow at the same temperature for 2 h.

Afterwards, the different mixtures were fed with a total reaction flow rate of 16.6 ml min^{-1}. For the dry reforming of methane, the [CH_4:CO_2:Ar] ratios were [1:1:1.2] and [1:1.9:0.3]. But for the combined reforming of methane, with the addition of 10% O_2 partially or totally replacing Ar, the [CH_4:CO_2:O_2:Ar] ratios were [1:1:0.3:0.9] and [1:1.9:0.3:0].

The conversions were measured after a 1-h stabilization period. The reaction products and the permeated mixture for both reactor types were analyzed with two on-line thermal conductivity detector gas chromatographs: a Shimadzu GC-8A and a SRI 8610C (SRI Instruments (USA)). The former instrument was equipped with a Porapak column, and the latter with a molecular sieve column. The carbon balance was close to one in all cases.

2.3.3. Thermodynamic calculations

The HYSYS software package (HyproTech.HYSYS.Process.v2.2 AEA Technology) was used for simulation purposes of a Gibbs reactor. The Peng–Robinson equations of state were used to calculate the stream properties. To calculate the data, we employed the same total flow used in laboratory experiments. Even the dimensions given to the Gibbs reactor were equal to those used in the laboratory.

3. Results and discussion

3.1. Methane turnover frequencies and proposed model for Ru supported on binary La_2O_3–SiO_2 solids

The activity and stability of a series of Ru catalysts were previously evaluated in a differential fixed-bed reactor for the dry reforming of methane reaction [16]. Table 1 shows the metallic dispersion, forward turnover frequency values (TOF), particle sizes and

Table 1
Forward methane turnover frequency, H_2/CO ratio, dispersion and particle size for Ru/La_2O_3–SiO_2 catalysts after different reduction temperatures.

Solids[a]	D (%)[b]	TOF_{CH_4} (s^{-1})[c]	dp (nm)	H_2/CO ratio
$Ru/La_2O_3(15)$–SiO_2	36	4.42	2.50	0.27
$Ru/La_2O_3(27)$–SiO_2	24	4.09	3.75	0.26
$Ru/La_2O_3(40)$–SiO_2	29	2.90	3.11	0.37
$Ru/La_2O_3(50)$–SiO_2	36	5.20	2.50	0.36

[a] The wt.% of La_2O_3 is indicated between parentheses. All solids contain 0.6 wt.% of Ru. The catalysts were reduced in flowing H_2 at 550 °C.
[b] The Ru dispersion was calculated from CO chemisorption at room temperature, assuming that the CO/Ru ratio was equal to 1.
[c] $P_{CO_2} : P_{CH_4} : P_{Ar} = 1 : 1 : 1.2$, $P = 101$ kPa, $W/F = 4.5 \times 10^{-6}$ g h ml^{-1}, $T = 550$ °C.

Table 2
Catalytic behavior in a conventional fixed-bed reactor for different feed compositions.

CO_2:CH_4:O_2:Ar	X_{CH_4} [a]	X_{CO_2} [a]	H_2/COth [b]	H_2/CO	X_{CH_4} [c] HYSYS	X_{CO_2} [c] HYSYS
1:1:0:1.2	29.4	42.1	0.65	0.68	30.7	41.6
1:1:0.3:0.9	43.3	14.8	–	1.11	47.2	12.5
1.9:1:0:0.3	34.2	30.3	0.49	0.56	37.8	31.2
1.9:1:0.3:0	50.6	15.1	–	0.80	51.9	14.2

[a] Methane and carbon dioxide conversions, catalyst mass = 0.2 g, $W/F = 2 \times 10^{-4}$ g h ml^{-1}, reaction temperature = 550 °C.
[b] Calculated from $H_2/CO = (3 - (x_{CO_2}/x_{CH_4}))/(1 + (x_{CO_2}/x_{CH_4}))$.
[c] Calculated using HYSYS software.

measured H_2/CO ratios. All catalysts exhibited high reaction rates and were stable after 100 h on stream.

In order to check the differential conditions, the forward reaction rates (r_f) were calculated from the net rate of reaction (r_n). The r_f can be estimated as follows:

$$r_f = r_n(1-\eta) \quad \eta = \frac{(P_{CO})^2(P_{H_2})^2}{P_{CH_4}P_{CO_2}}\frac{1}{Ke}$$

where P_is are the prevalent pressures of reactants and products and *Ke* is the equilibrium constant calculated at the corresponding reaction temperature. The calculated η values were lower than 0.0002 confirming the quality of the differential data obtained.

The lowest TOF was observed for the Ru/La_2O_3(40)–SiO_2 catalyst reduced at 550 °C. The low lanthanum content solids exhibited similar TOF_{CH_4} values (TOF = 4.4 ± 0.3) independently of the reduction temperature. Table 1 shows that there is no relationship between dispersion and TOF with the increase of the La_2O_3 load. Note that for all catalysts, the same Ru content was employed.

When Ru and other noble metals are supported on non-carbonate forming oxides such as Al_2O_3 or SiO_2, Wei and Iglesia [17] found that forward CH_4 turnover rates increased with increasing Ru dispersion. For these catalysts, they showed that the reaction kinetics are first-order in methane and zero order in CO_2 partial pressures. However, for Rh/La_2O_3 catalysts, the CO_2 reaction order varies between 0.37 and 0.50. This is symptomatic of the strong interaction between CO_2 and La_2O_3 which is reflected in the formation of oxycarbonates at the surface and the bulk level, at least after being exposed to the reacting mixture. In the case of Rh/La_2O_3(27)–SiO_2, the proportion of oxycarbonate formed was much lower mainly due to the presence of lanthanum disilicate which restricted the amount of La_2O_3 available to react with CO_2 [18].

A complete physicochemical characterization was published in a previous work [16]. Taking into account the formation of a surface layer of lanthanum disilicate and the influence of lanthanum upon the Ru particle size and the metal–support interaction, we proposed a model for the Ru/La_2O_3–SiO_2 system [16].

The XPS and ISS results indicated that the full coverage by a lanthanum disilicate layer occurred at 40 wt.% of La_2O_3. When the support contained 50 wt.% of La_2O_3, LaO_x particles appeared and a strong Ru–support interaction was revealed by both XPS and TPR. On the basis of these results, we can speculate that the LaO_x formed after the catalyst reduction partially covered the Ru particle, leading to a decrease in the CO chemisorption.

The Ru/La_2O_3(50)–SiO_2 catalyst showed the highest TOF suggesting that more reactive particles were present when a strong Ru–La interaction was observed. For this reason, this catalyst was applied in a membrane reactor for the dry reforming reaction combined with methane oxidation reactions.

3.2. Catalytic behavior of Ru/La_2O_3(50)–SiO_2 in the conventional fixed-bed reactor for combined reforming

As a starting point, the catalyst was evaluated for combined methane reforming in a reactor with a bed height of 0.8 cm to simulate the bed which was then placed above the membrane in the membrane reactor to avoid oxygen exposure of the Pd–Ag alloy. The catalyst was evaluated using the same total flow that was employed in the membrane reactor and several feed compositions to increase both the conversion of CH_4 and H_2 production.

Table 2 shows the methane and carbon dioxide conversions and the H_2/CO ratio for the dry and combined reforming of methane. The methane conversion increases when the CO_2/CH_4 ratio increases from 1.0 to 1.9. When oxygen is added to the feed stream (CRM), the conversion of methane increases while that of carbon dioxide decreases due to the occurrence of the total oxidation of methane.

The H_2/CO ratios are higher when the CO_2/CH_4 ratio is equal to 1. It can be clearly seen that as long as the CO_2/CH_4 ratio in the reactant mixture increases, H_2 selectivity and H_2/CO ratio decay. The CO_2 excess in the reactant mixture with respect to the stoichiometric ratio of the dry reforming reaction ($CH_4 + CO_2 \rightleftarrows 2H_2 + 2CO$) favors the occurrence of the reverse water gas shift (RWGS) reaction ($CO_2 + H_2 \rightleftarrows CO + H_2O$). This secondary process consuming CO_2 and the produced H_2 leads to a decrease in the H_2/CO ratio in the outlet stream while producing H_2O in the reaction medium. The theoretical values of these ratios for the dry reforming are similar to those chromatographically measured.

For the case of combined reforming, as a consequence of the occurrence of both reactions ($CH_4 + CO_2 \rightleftarrows 2H_2 + 2CO$ and $CH_4 + (1/2)O_2 \rightleftarrows 2H_2 + CO$), a higher H_2/CO ratio was obtained, in agreement with what has been reported by other authors [19,20].

In our previous work [13], we optimized the amount of oxygen in the feed stream. The Rh/La_2O_3–SiO_2 catalyst yielded the best results for combined reforming with an oxygen concentration of 10%, compared with lower values (3 and 6% O_2). In the case of the addition of oxygen to the feed mixture, the reactions that might occur are partial oxidation of methane (POM) and dry reforming reaction (DRM) in addition to total oxidation of methane ($CH_4 + 2O_2 \rightleftarrows 2H_2O + CO_2$) and the reverse (RWGS) or direct water gas shift reaction. In the reactor outlet, oxygen was not chromatographically detected, indicating that it was completely consumed in the 0.8 cm catalytic bed.

Parallel to the experimental study, a theoretical analysis of the effect of the CO_2/CH_4 ratio in the feed mixture was performed. The dry and combined reforming of methane was investigated making thermodynamic equilibrium calculations (Gibbs reactor) in the given chemical system as a function of the CO_2/CH_4 ratio.

In previous reports, Ávila-Neto et al. [21] conducted a comparative and complete analysis of methane reforming reactions to asses the influence of key operational variables on chemical equilibrium. Among all the variables studied, they analyzed the effect of CO_2/CH_4 ratio for a temperature of 1000 °C. On the other hand, Amin and Yaw [22] analyzed the effect of CH_4:CO_2:O_2 feed ratios and the operating temperatures on the combined reforming of methane with carbon

dioxide and the partial oxidation of methane process by means of total Gibbs energy minimization of the system. In the latter work, the authors studied CO_2/CH_4 ratios lower than unity.

To calculate the data, we employed the same total flow and compositions used in laboratory experiments. Even the dimensions given to the Gibbs reactor were equal to those used in the laboratory.

From our simulated data, methane and carbon dioxide conversions, the H_2/CO and the produced H_2/fed CH_4 ratios were calculated for the different feed conditions employed in the membrane reactor. These values were plotted as a function of the CO_2/CH_4 ratio in the feed (Fig. 1a and b).

In the case of dry reforming, as the CO_2/CH_4 ratio increased, the methane conversion also increased whereas the CO_2 conversion and H_2/CO ratio decreased. However, the produced H_2/fed CH_4 ratio presented the highest value when a CO_2/CH_4 ratio above the stoichiometric value was used.

For combined reforming, the methane and CO_2 conversions slightly increased, the produced H_2/fed CH_4 ratio remained practically constant for the range of concentrations studied, while the H_2/CO ratio decreased. Therefore, this theoretical study shows that the most favorable conditions to evaluate the Ru/La_2O_3–SiO_2 catalyst are CO_2/CH_4 ratios between 1 and 1.9 for both, dry and combined reforming reactions.

Theoretical conversion values calculated by HYSYS are close to those experimentally obtained (Table 2). These findings indicate that with a 0.8 cm catalyst bed, the system is in thermodynamic equilibrium. Thus, it is concluded that the role of the catalytic bed in contact with the membrane would be to restore the thermodynamic equilibrium since hydrogen is extracted from the reaction system continuously.

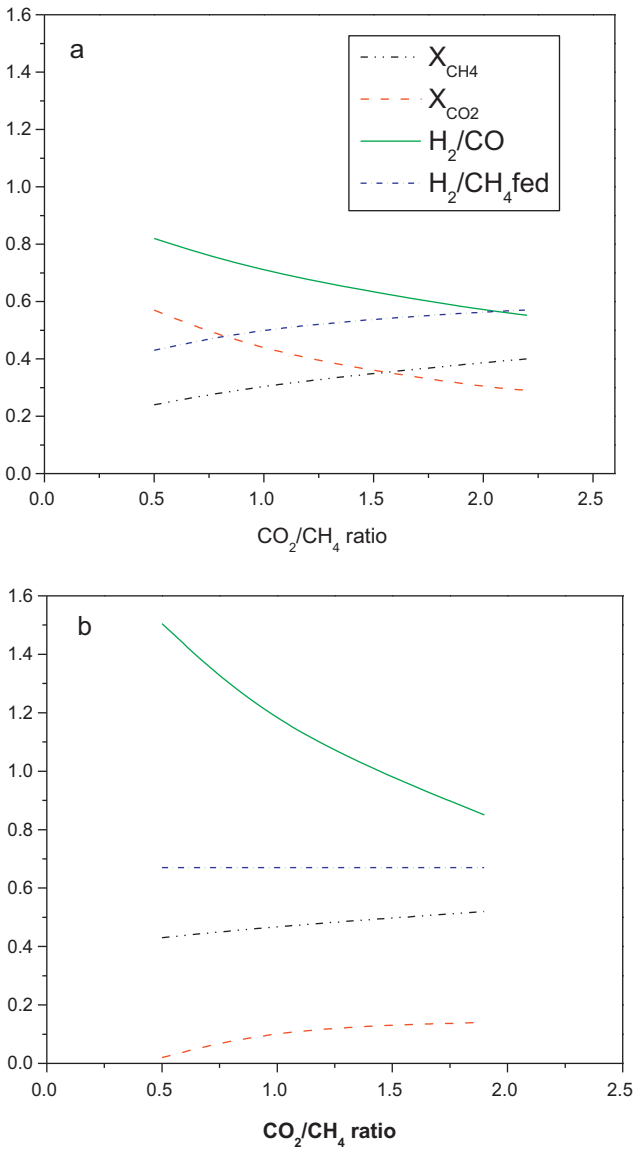

Fig. 1. Methane (X_{CH_4}) and carbon dioxide (X_{CO_2}) conversions, H_2/CO ratio and produced H_2/CH_4 fed ratio as a function of the CO_2/CH_4 reactant ratio. Theoretical values calculated using HYSYS 3.0.1. Total flow = 16.6 ml min^{-1}. (a) Without oxygen and (b) with 10% of oxygen in the feed mixture.

3.3. Catalytic behavior of $Ru/La_2O_3(50)$–SiO_2 in the membrane reactor

3.3.1. Membrane characterization

The transport capacity of hydrogen through the palladium membrane is generally quantified in terms of permeability, permeance or permeation flow. The flow of atomic hydrogen through the Pd membrane is the product of the diffusion coefficient and concentration gradient. The concentration of H atoms in the Pd may be related to the partial pressure of the gas, while the permeation flux (J) is expressed by Sievert's law.

$$J = \frac{P_{er}\left(\left(\sqrt{PH_2}\right)_1 - \left(\sqrt{PH_2}\right)_2\right)}{l} \quad (1)$$

The value of $n = 0.5$, as an exponent of the different pressures $[(P_1)^{0.5} - (P_2)^{0.5}]$, would indicate that the rate determining step is the diffusion of H atoms through the metal film. The permeability of H_2 (P_e) was determined at different temperatures for the two membranes studied. The dependence of permeability with temperature was adjusted according to the Arrhenius law.

$$P_e = P_o e^{-(E/RT)} \quad (2)$$

where P_o is the pre-exponential factor [mol m^{-1} s^{-1} $Pa^{-0.5}$], E is the activation energy of H_2 transport through the membrane, R is the gas constant and T is temperature in K.

A plot of ln(P_e) vs 1000/T is shown in Fig. 2. The apparent activation energies calculated from the slopes are 11 and 24 kJ/mol, while the pre-exponential factors calculated from the intercepts are 1.99×10^{-6} and 5.55×10^{-5} mol m^{-1} s^{-1} $Pa^{-0.5}$ for the M1 and

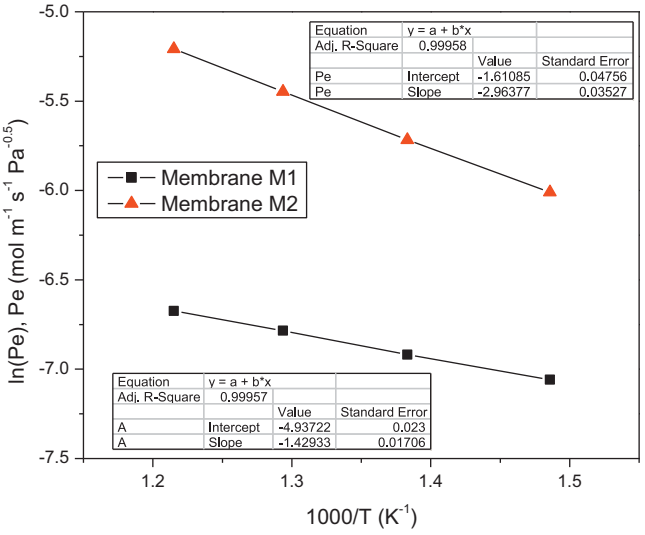

Fig. 2. Permeability as a function of temperature for the M1 and M2 membranes (trans-membrane pressure of 20 kPa).

Table 3
Comparison between the two Pd–Ag membranes (M1 and M2).

SG (ml min^{-1})	H_2 recovery				Permeated H_2 flow rate (ml min^{-1})			
	DRM[a]		CRM[a]		DRM[a]		CRM[a]	
	M1	M2	M1	M2	M1	M2	M1	M2
10	0.35	0.36	0.32	0.38	0.99	1.04	1.22	1.53
30	0.49	0.62	0.44	0.63	1.69	2.26	1.82	3.14
50	0.55	0.73	0.49	0.72	1.80	2.82	2.08	3.85
70	0.55	0.77	0.53	0.77	1.89	2.99	2.36	4.20

[a] $CO_2/CH_4 = 1$, catalyst mass = 1.5 g, $W/F = 1.5 \times 10^{-3}$ g h ml^{-1}, $P = 101$ kPa, $T = 550$ °C, and permeation area = 4 cm^2.

M2 membranes, respectively. The expressions that allow determining permeability as a function of temperature for the membranes under study are the following:

$$P_e = 1.99 \times 10^{-6} \times \exp\left(\frac{-(11\ \text{kJ/mol})}{RT}\right) \quad \text{M1 membrane} \qquad (3)$$

$$P_e = 5.55 \times 10^{-5} \times \exp\left(\frac{-(24\ \text{kJ/mol})}{RT}\right) \quad \text{M2 membrane} \qquad (4)$$

The relative magnitude of both the activation energy and the pre-exponential factor obtained in this work show similar values to those reported in the literature for Pd–Ag membranes with a several-micron thickness [23]. Membrane M2 exhibits a higher permeation flow than the M1 membrane (Fig. 2). At 550 °C and a trans-membrane pressure of 50 kPa, no He flux through the membrane was observed. This implied the absence of defects in the metal film or sealing leaks and assured 100% selectivity to hydrogen.

3.3.2. *Performance of the membrane reactors built with two different Pd–Ag membranes*

Table 3 shows the H_2 recovery (H_2 permeated/H_2 produced) and H_2 flow values for the Ru/La_2O_3(50)–SiO_2 catalyst employing both membranes, M1 and M2, and two different feeds (DRM and CRM). The same bed height, i.e., the same area of permeation was used for both membranes. It can be observed that the permeation flux and H_2 recovery are higher for membrane M2 when the comparison is performed at the same SG flow rate. The H_2 recovery is about 77% for M2, while a value of 55% is obtained for M1 for a SG flow rate of 70 ml min^{-1}. Note that for two different reaction systems, DRM and CRM, the H_2 recovery is dependent on the membrane employed. For each membrane, the same values of hydrogen recovery are obtained under DRM and CRM conditions at the same SG flow rate. Besides, higher permeated hydrogen flows are observed for the combined reforming of methane. The addition of O_2 not only increases the methane conversion but it also increases the hydrogen production (Fig. 1) thus increasing the driving force for hydrogen permeation.

To describe the optimal operation of membrane reactors, different approaches have been reported in the literature [24–26]. In general, we need to balance the feed flow rate, the reaction rate and the permeation flow. A key factor is the catalyst ability to restore the chemical equilibrium upon H_2 withdrawal; besides, the permeation flux must be high enough to eliminate as much H_2 produced as possible.

An equilibrium fraction of the dry reforming reaction of methane can be defined, which shows the approach to equilibrium of this reaction [4,25,26]:

$$\eta = \frac{\prod_i p_i^{vi}}{K_{eq}} \qquad (5)$$

where *pi* is the partial pressure of each reactant and product in the reaction side of the membrane reactor, *vi* is the DRM stoichiometric number, and K_{eq} is the equilibrium constant (evaluated in the fixed-bed reactor, which is close to the theoretical value). If the composition corresponds to thermodynamic equilibrium, this ratio is equal to 1.

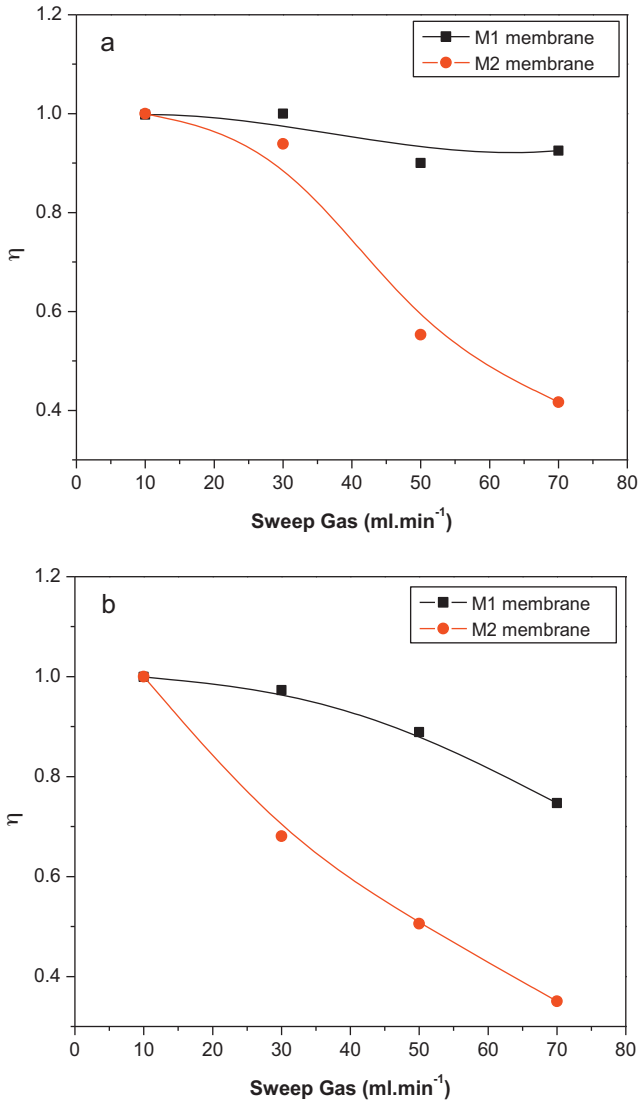

Fig. 3. Ability of the catalyst to keep the retentate equilibrated when the membrane reactor was built with M1 and M2 membranes as a function of the sweep gas flow rate (SG): (a) for DRM and (b) for CRM. $T = 550$ °C, $\Delta P = 0$, catalyst mass = 1.5 g, $W/F = 1.5 \times 10^{-3}$ g h ml^{-1}.

The η values calculated for the different feed conditions are shown in Fig. 3a and b. Note that η remains practically constant and close to 1 for the case of membrane M1 for the dry reforming of methane. While for membrane M2, η starts from unit and, when the SG flow rate is higher than 30 ml min^{-1}, the η value decreases indicating that when high H_2 flow is removed from the system, the catalyst cannot restore the equilibrium. A more active catalyst

should be developed to balance the reaction rate and the permeation flow.

In the case of the CRM reaction, the same behavior is observed but even more pronounced. For M1 a η value of 0.8 is obtained for a SG flow of 70 ml min^{-1} while for M2 the value is below 0.4. Comparing both reaction systems, employing the same membrane and catalyst, the main difference is present in the gas composition that reaches the catalytic bed in the membrane reactor. This composition could influence the ability of the catalyst to restore the equilibrium.

Fig. 4a and b shows the H_2 partial pressure on both sides of the membrane (permeate and retentate) as a function of sweep gas flow rates (SG) for DRM and for the two membranes under study. In the case of the M1 membrane at SG flow rate of 70 ml min^{-1}, the H_2 partial pressure in the retentate side is approximately equal to 9 kPa while in the permeate side it is less than ~3 kPa. However, the H_2 partial pressure on both sides of the M2 membrane presents a different behavior. The retentate and permeate H_2 partial pressures decrease as the sweep gas flow rate increases, maintaining a nearly constant difference between them. For a sweep gas of

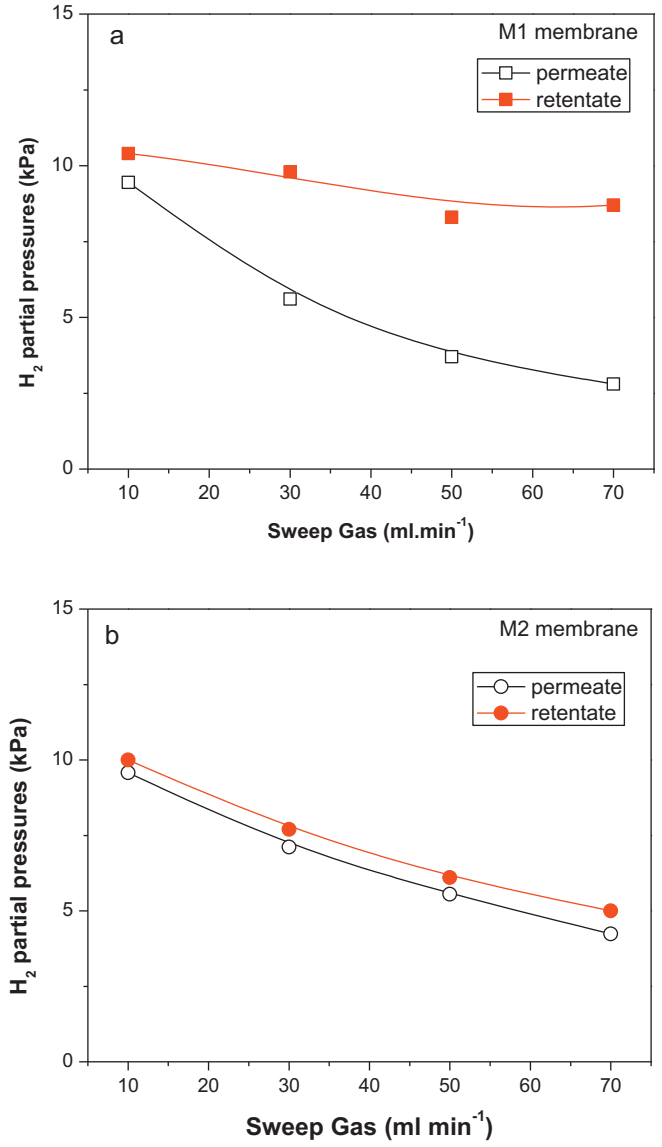

Fig. 4. H_2 partial pressures on both sides of the membranes as a function of sweep gas under DRM conditions: (a) M1 membrane and (b) M2 membrane. T = 550 °C, ΔP = 0, W = 1.5 g, W/F = 1.5 × 10^{-3} g h ml^{-1}.

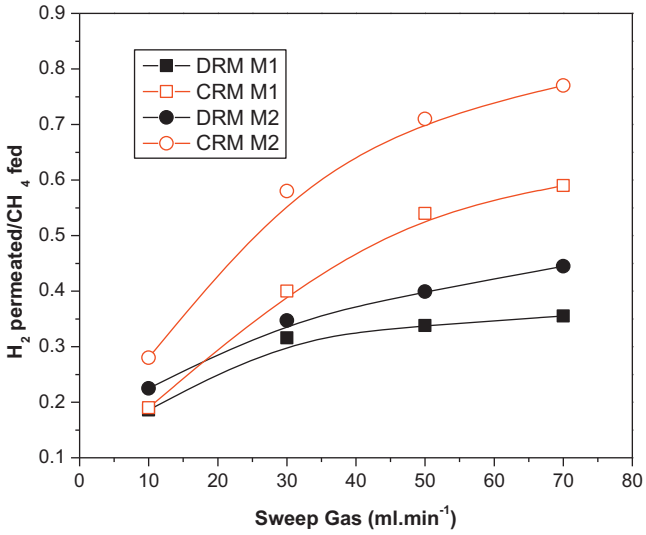

Fig. 5. H_2 permeated/CH_4 fed ratio as a function of sweep gas for two membranes (M1 and M2). Permeation area = 4 cm^2. T = 550 °C, ΔP = 0, catalyst mass = 1.5 g, W/F = 1.5 × 10^{-3} g h ml^{-1}.

70 ml min^{-1}, H_2 partial pressures of 5 kPa and 4.2 kPa are obtained in the retentate and the permeate sides of the membrane reactor, respectively. These results suggest that in the case of the M1 membrane, the hydrogen flow would be the limiting factor in the membrane reactor.

Due to the occurrence of both reactions (DRM and partial oxidation), higher H_2 permeated/CH_4 fed ratios are obtained under CRM conditions employing M1 or M2 membranes.

With both membranes studied, similar methane conversion values are obtained (not shown). However, when compared to the same feed condition, higher values of H_2 permeated/CH_4 fed ratios are obtained for the M2 membrane (Fig. 5).

For the above reason, this membrane was selected to study the effect of permeation area and reactant ratio on the performance of a membrane reactor operating with the Ru/La_2O_3(50)–SiO_2 catalyst. Tong and Matsumura studied two alumina-supported nickel catalysts in a hydrogen-permeable membrane reactor [27]. They concluded that the separation of hydrogen through the palladium membrane shifts the equilibrium to the larger conversion of methane, but the less active catalyst produces a lower conversion than the values expected from the shifted equilibrium, which depends on the hydrogen recovery. The higher space velocity of the reactant results in a lower conversion in the membrane reactor, mainly because the hydrogen separation ratio decreases with an increase in the space velocity. The active catalyst produces the methane conversion close to the equilibrium expected from the hydrogen separation ratio at the reactor exit. Consequently, the catalytic activity also affects the hydrogen flux through the membrane.

3.3.3. *Effect of the permeation area*

Table 4 shows the influence of the permeation area on the performance of Ru/La_2O_3(50)–SiO_2 for the dry reforming reaction and the combined reaction with a CO_2/CH_4 = 1. The catalyst was evaluated using 4 and 6 cm^2 permeation area. The catalyst mass was 1.5 g and it was diluted with 8 g of quartz to obtain a permeation area of 4 cm^2 and 10 g of quartz for 6 cm^2. With this diluted catalyst mass, it was possible to reach the permeation area required plus 0.8 cm of catalyst bed above the membrane.

The results are consistent with the expected behavior, i.e., when the permeation area increases, the hydrogen permeate flow rate increases. Note that the H_2 recovery is similar for both conditions.

Table 4
Effect of the permeation area upon the performance of the M2 membrane reactor.

SG (ml min^{-1})	H_2 recovery				H_2 flow (ml min^{-1})			
	DRM[a]		CRM[a]		DRM[a]		CRM[a]	
	[b]A = 4 cm^2	A = 6 cm^2	A = 4 cm^2	A = 6 cm^2	A = 4cm^2	A = 6 cm^2	A = 4 cm^2	A = 6 cm^2
10	0.36	0.37	0.38	0.38	1.04	1.11	1.53	1.68
30	0.62	0.63	0.63	0.63	2.26	2.37	3.14	3.43
50	0.73	0.73	0.72	0.73	2.82	3.17	3.85	4.25
70	0.77	0.78	0.77	0.77	2.99	3.48	4.20	4.64
90	–	0.82	–	0.81	–	3.74	–	5.06
110	–	0.84	–	0.83	–	4.16	–	5.25
130	–	0.86	–	0.85	–	4.24	–	5.52

[a] CO_2/CH_4 = 1, catalyst mass = 1.5 g, $W/F = 1.5 \times 10^{-3}$ g h ml^{-1}, P = 101 kPa, T = 550 °C.
[b] A: permeation area.

Table 5
CH_4 and CO_2 conversions and produced H_2/CO ratios for $Ru/La_2O_3(50)–SiO_2$ catalyst in the M2 membrane reactor.

SG (ml min^{-1})	X_{CH_4}		X_{CO_2}		H_2/CO[b]		pH_2[c]	
	DRM[a]	CRM[a]	DRM[a]	CRM[a]	DRM[a]	CRM[a]	DRM[a]	CRM[a]
0	29.4	43.3	42.1	14.8	0.68	1.11	12.2	18.0
10	31.5	46.0	40.4	20.0	0.77	1.31	10.4	15.7
30	38.4	51.5	46.5	19.4	0.84	1.43	7.8	11.6
50	42.5	53.9	49.4	21.0	0.89	1.50	6.5	9.4
70	43.7	54.5	49.7	22.0	0.92	1.47	5.7	8.1
90	45.1	55.4	50.4	20.0	0.90	1.56	4.8	6.9
110	50.0	57.5	55.6	20.7	0.89	1.53	4.5	6.5
130	51.0	56.8	54.1	22.7	0.91	1.48	3.9	5.8

[a] CO_2/CH_4 = 1, permeation area = 6 cm^2, catalyst mass = 1.5 g, $W/F = 1.5 \times 10^{-3}$ g h ml^{-1}, P = 101 kPa, T = 550 °C.
[b] Total hydrogen (retentate + permeated)/CO ratio.
[c] Retentate hydrogen partial pressure (kPa).

This behavior could be explained through the relationship between the H_2 recovery and the inverse Damköhler–Peclet product. This quantity is defined by 1/DaPe = (maximum permeation rate per volume)/(maximum reaction rate per volume) and it could be derived from the definition of the Damköhler and Peclet numbers, yielding the following equation:

$$\frac{1}{\mathrm{Da}\cdot\mathrm{Pe}} = \frac{Q\cdot A_m}{A_c\cdot L\cdot \rho_{cat}\cdot k} \quad (6)$$

where Q is the product permeance, A_m the membrane area, A_c the cross-sectional area of the bed, L catalyst bed length, ρ_{cat} catalyst density and k the reaction rate constant. The following assumptions are made to derive the above equation: no radial gradients are present, the reaction rate is first-order, the permeation rate is linear in pressure difference, and the total pressure in the reactant and permeate sides is the same.

In previous papers, Oyama and coworkers [28] defined an Operability Level Coefficient (OLC) as the ratio of the actual permeation rate and the actual formation rate of a critical product in a membrane reactor, in this case the critical product being hydrogen. The authors claimed that for this type of membrane reactors, the OLC could be defined in terms of the Da and Pe numbers evaluated at the reaction conditions ($\mathrm{OLC} = (1/\mathrm{DaPe})_{\text{reaction conditions}}$).

This coefficient is equivalent to the hydrogen recovery parameter defined as H_2 permeated/H_2 produced ratio for a given condition (sweep gas flow rate, reaction temperature, feed composition, catalytic system, membrane permeance, etc.). In the same way, the hydrogen recovery is related to the inverse Damköhler–Peclet product.

When the permeation area ($A_m = \pi \times \mathrm{Diameter} \times \mathrm{Length}$) is increased, the catalyst bed length increases and there is no effect on the hydrogen recovery.

For the highest permeation area, the measurements were carried out at higher sweep gas flow rates, resulting in a H_2 flow of 4.24 and 5.52 ml min^{-1} for the DRM and CRM, respectively, and a recovery of 86% H_2 in both cases (Table 4). From these results, we selected the higher permeation area (6 cm^2) for the following measurements.

3.3.4. *Effect of CO_2/CH_4 ratio on hydrogen production*

Table 5 shows the influence of the sweep gas flow rate on the conversion of methane and carbon dioxide for DRM and CRM using a CO_2/CH_4 ratio equal to 1. The evaluation in the fixed-bed reactor is equivalent to that of the membrane reactor with SG flow equal to zero. The conversions reach the theoretical equilibrium values (Table 2). When the SG increases, conversions exceed these values and the difference between the conversion of CH_4 and CO_2 decreases for DRM. Besides, the produced H_2/CO ratio approaches 1. These results suggest that the hydrogen separation in the membrane reactor is unfavorable for the RWGS reaction. This could be a consequence of the lower partial pressure of hydrogen in the reaction zone that reduces the RWGS rate. It is further noted that the conversions of both CH_4 and CO_2 increase with increasing of SG flow rate. In the case of the addition of oxygen to the feed mixture (CRM), the reactions that might occur in the 0.8 cm of catalytic bed are partial oxidation of methane and dry reforming reaction in addition to the reverse or direct water gas shift reaction and total oxidation of methane. As a consequence of these reactions, the carbon dioxide conversion is significantly lower than the methane conversion and the H_2/CO ratio is much higher than 1 (Fig. 1).

Fig. 6 shows the methane conversion as a function of the sweep gas flow rate for different feed conditions. Similarly to what is observed in the fixed-bed reactor (Table 2), methane conversion increases when the CO_2/CH_4 ratio increases from 1.0 to 1.9 and when oxygen is added to the feed mixture. For the case where the CO_2/CH_4 ratio is equal to 1.9, a difference of approximately 10% conversion between DRM and CRM always remains, for all the sweep gas conditions studied. For SG flow rates over 50 ml min^{-1}, the conversions of both CH_4 and CO_2 remain roughly constant except for the case of DRM in the CO_2/CH_4 ratio equal to 1.

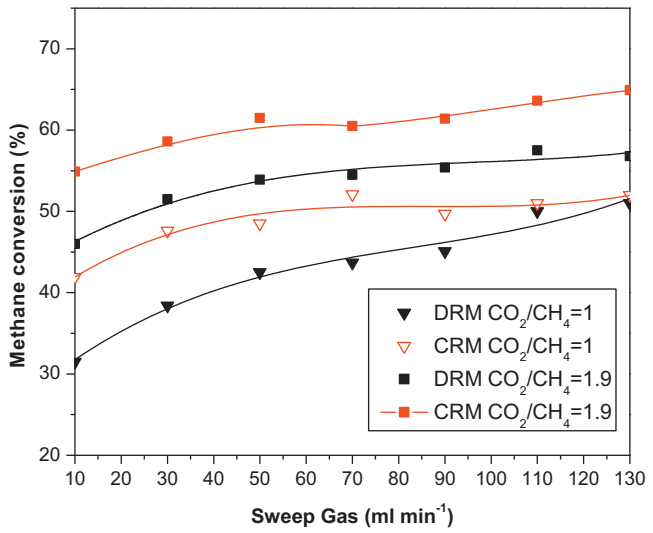

Fig. 6. CH_4 conversion as a function of sweep gas flow rate. To vary the CO_2/CH_4 ratio the following CH_4:CO_2:Ar ratios were employed: [1:1:1.2] and [1:1.9:0.3] and with 10% of O_2 the CH_4:CO_2:O_2:Ar ratios were [1:1:0.3:0.9] and [1:1.9:0.3:0]. Membrane: M2, permeation area = 6 cm^2, T = 550 °C, ΔP = 0, W = 1.5 g, $W/F = 1.5 \times 10^{-3}$ g h ml^{-1}.

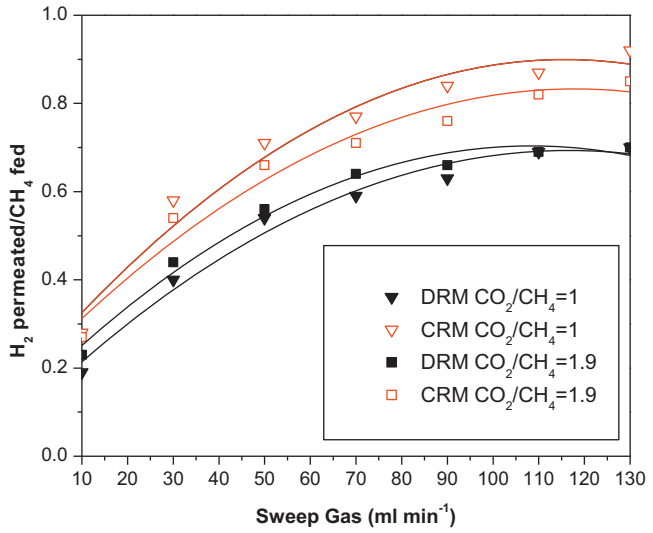

Fig. 7. H_2 permeated/CH_4 fed as a function of sweep gas for the different feed mixtures under DRM and CRM conditions. Membrane: M2, permeation area = 6 cm^2, T = 550 °C, ΔP = 0, W = 1.5 g, $W/F = 1.5 \times 10^{-3}$ g h ml^{-1}.

Fig. 7 shows the H_2 permeated/CH_4 fed ratio as a function of the sweep gas. The CRM curves are always above those of DRM. This means that the operating conditions of CRM not only yield a considerable increase in conversion but also result in an increased production of hydrogen. When the sweep gas flow rate increases, the retentate hydrogen partial pressure is always higher for the CRM reaction system comparing to the DRM conditions. The results for CO_2/CH_4 ratio = 1 are shown in Table 5. The same behavior was observed when this ratio was equal to 1.9.

Ferreira-Aparicio et al. [5] reported data using a highly selective Pd membrane (12–35 μm) supported on porous stainless steel and various Ni-based catalysts in a membrane reactor for the dry reforming reaction. They found that excess CO_2 in the feed with respect to the stoichiometric ratio provides more favorable conditions for the operation of membrane reactors. However, the CO_2 surplus in the feed must be limited to a certain level to reduce H_2O formation as much as possible through the RWGS, given the fact that the hydrogen recovery yield decreases when the CO_2/CH_4 ratio becomes too high. Under these conditions, their system produces hydrogen permeation flux of 4.4×10^{-7} mol s^{-1} m^{-2} with a recovery of hydrogen (H_2 permeated/H_2 produced = 0.93) of 93% for CO_2/CH_4 ratio equal to 1.9 and 0.223 mmol s^{-1} of SG. However, we obtained a higher flow of H_2 equal to 1.35×10^{-6} mol s^{-1} m^{-2} and a hydrogen recovery of 86% for a CO_2/CH_4 ratio equal to 1 with 0.1 mmol s^{-1} of SG (130 ml min^{-1}).

For CO_2/CH_4 ratios higher than the stoichiometric ratio (CO_2/CH_4 = 1.9), a slightly lower flow was obtained. The H_2 permeation flow was 1.23×10^{-6} mol s^{-1} m^{-2} for a SG flow rate of 0.1 mmol s^{-1} (130 ml min^{-1}). This behavior could be due to the catalyst deactivation produced by the reoxidation of metallic Ru when it is in contact with carbon dioxide rich streams. We have previously studied this effect on Ru/La catalysts by in situ Raman experiments [18]. The oxidation of Ru/La_2O_3 catalysts in CO_2 pulses was also reported by Matsui et al. [29]. They studied the effect of the support on the activities and mechanisms in the CO_2 reforming of methane over Ru catalysts. Over Ru/La_2O_3 catalysts they proposed the following reaction step based on pulse experiments:

$$Ru/La_2O_3 + CO_2(ad) \Rightarrow CO(gas) + Ru\text{–}Ox/La_2O_3$$

In addition, the ruthenium re-oxidation was consistent with the observation of Yan et al. [30]. They reported a significant catalytic difference between Rh/SiO_2 and Ru/SiO_2 which was attributed to the great differences in the Rh–O (405.0 kJ/mol) and Ru–O (528.4 kJ/mol) bond strengths. This renders the reduction of Ru/SiO_2 more difficult than that of Rh/SiO_2. However, Múnera et al. [31] for the Rh/La_2O_3 system, did not observe any deactivation at high P_{CO_2}/P_{CH_4} ratios.

4. Conclusions

La_2O_3–SiO_2 binary supports with different La loadings allowed us to obtain active, stable and high dispersion Ru catalysts for the dry reforming reaction of methane. Through the combined use of a battery of techniques, information on the distribution of lanthanum in the support was obtained and reported previously [16].

The catalyst with the highest load of lanthanum, $Ru/La_2O_3(50)$–SiO_2, exhibited the highest value of TOF_{CH_4}, with a Ru dispersion of 38% (Table 1). The performance of this catalyst was evaluated in a membrane reactor for the reforming of methane, using two different Pd–Ag membranes. The reactor configuration applied was formed by a fixed-bed reactor followed by a membrane reactor. Using either the M1 or M2 membrane, the reactor performance was limited by the permeability of the membrane. The H_2 recovery remained constant when the membrane permeation area increased since the catalyst bed also increased in the same proportion.

A bed height of 0.8 cm above the membrane was enough to react the 10% O_2 fed during the CRM avoiding the damaging effect of oxygen on the Pd alloy. From there on, the role of the catalyst was to roughly maintain the retentate side equilibrated while hydrogen permeated out of the shell side of the membrane reactor.

Under CRM the methane conversion increased compared to those obtained in DRM. Besides, by increasing the CO_2/CH_4 ratio from 1 to 1.9, the methane conversion increased.

Acknowledgements

The authors wish to acknowledge the financial support received from UNL, ANPCyT and CONICET. Thanks are also to Prof. Elsa Grimaldi for the English language editing.

References

[1] M. Bradford, M. Vannice, Catal. Rev. Sci. Eng. 41 (1999) 1–42.
[2] K. Nagaoka, M. Okamura, K. Aika, Catal. Commun. 2 (2001) 255–260.
[3] B. Faroldi, C. Carrara, E.A. Lombardo, L. Cornaglia, Appl. Catal. A: Gen. 319 (2007) 38–46.
[4] S. Irusta, J. Múnera, C. Carrara, E.A. Lombardo, L.M. Cornaglia, Appl. Catal. A: Gen. 287 (2005) 147–158.
[5] P. Ferreira-Aparicio, M. Benito, S. Menad, J. Catal. 231 (2005) 331–343.
[6] D. Lee, P. Hacarlioglu, S.T. Oyama, Top. Catal. 29 (2004) 45–57.
[7] J.F. Múnera, L. Coronel, B. Faroldi, C. Carrara, E. Lombardo, L. Cornaglia, Asia-Pac. J. Chem. Eng. 5 (1) (2010) 35–47.
[8] C. Carrara, A. Roa, L. Cornaglia, E. Lombardo, C. Mateos-Pedrero, P. Ruiz, Catal. Today 133–135 (1–4) (2008) 344–350.
[9] E. Ruckenstein, H. Yun Hang, Appl. Catal. A: Gen. 154 (1997) 185–205.
[10] L. Mo, X. Zheng, Q. Jing, H. Lou, J. Fei, Energy Fuels 19 (2005) 49–53.
[11] Q.S. Jing, X.M. Zheng, Energy Fuels 31 (2006) 2184–2192.
[12] M.M.V.M. Souza, M. Schmal, Appl. Catal. A: Gen. 281 (2005) 19–24.
[13] J.F. Múnera, C. Carrara, L.M. Cornaglia, E.A. Lombardo, Chem. Eng. J. 161 (2010) 204–211.
[14] H.-F. Chang, W.-J. Pai, Y.-J. Chen, W.-H. Lin, Int. J. HydrogenEnergy 35 (2010) 12986–12992.
[15] M. Simeone, L. Salemme, C. Allouis, Int. J. Hydrogen Energy 33 (2008) 4798–4808.
[16] B.M. Faroldi, E.A. Lombardo, L.M. Cornaglia, Appl. Catal. A: Gen. 369 (2009) 15–26.
[17] J. Wei, E. Iglesia, J. Phys. Chem. B 108 (2004) 7253–7262.
[18] C. Carrara, J. Múnera, E. Lombardo, L. Cornaglia, Top. Catal. 51 (2008) 98–106.
[19] M.M.V.V. Souza, M. Schmal, Appl. Catal. A: Gen. 225 (2003) 83–92.
[20] W. Wang, S.M. Stagg-Williams, F.B. Noronha, L.V. Mattos, F.B. Passos, Catal. Today 98 (2004) 553–563.
[21] C.N. Ávila-Neto, S.C. Dantas, F.A. Silva, T.V. Franco, L.L. Romanielo, C.E. Hori, A.J. Assis, J. Nat. Gas Sci. Eng. 1 (2009) 205–215.
[22] N.A.S. Amin, T.C. Yaw, Int. J. Hydrogen Energy 32 (2007) 1789–1798.
[23] V. Jayaraman, Y. Lin, J. Membr. Sci. 99 (1995) 251.
[24] C. Reo, L. Bernstein, C. Lund, Chem. Eng. Sci. 52 (1997) 3075–3083.
[25] L. Li, R. Borry, E. Iglesia, Chem. Eng. Sci. 57 (2002) 4595–4604.
[26] D. Ma, C.R.F. Lund, Ind. Eng. Chem. Res. 42 (2003) 711–717.
[27] J. Tong, Y. Matsumura, Appl. Catal. A: Gen. 286 (2005) 226–231.
[28] S.T. Oyama, H. Lim, Chem. Eng. J. 151 (2009) 351–358.
[29] N. Matsui, K. Anzai, N. Akamatsu, K. Nakagawa, N. Ikenaga, T. Suzuki, Appl. Catal. A: Gen. 179 (1999) 247–256.
[30] G. Yan, T. Wu, W. Weng, H. Toghiani, R.K. Toghiani, H.L. Wan, C.U. Pittman, J. Catal. 226 (2004) 247–259.
[31] J.F. Múnera, S. Irusta, L.M. Cornaglia, E.A. Lombardo, D.V. Cesar, M. Schmal, J. Catal. 245 (2007) 25–34.